Journal of Applied Physics ARTICLE scitation.org/journal/jap

A unified thermionic and thermionic-field emission (TE–TFE) model for ideal Schottky reverse-bias leakage current

Cite as: J. Appl. Phys. **131**, 015702 (2022); doi: 10.1063/5.0070668
Submitted: 8 September 2021 · Accepted: 9 December 2021 ·
Published Online: 3 January 2022

W. Li,[1,a)] D. Jena,[1,2,3] and H. G. Xing[1,2,3]

AFFILIATIONS

[1]School of Electrical and Computer Engineering, Cornell University, Ithaca, New York 14853, USA
[2]Department of Materials Science and Engineering, Cornell University, Ithaca, New York 14853, USA
[3]Kavli Institute at Cornell for Nanoscale Science, Cornell University, Ithaca, New York 14853, USA

[a)]**Author to whom correspondence should be addressed:** wl552@cornell.edu

ABSTRACT

We present a unified thermionic emission (TE) and thermionic-field emission (TFE) model for the ideal reverse-bias leakage current in Schottky junctions. The unified TE–TFE analytical model advances upon previous analytical TFE models by Murphy–Good and Padovani–Stratton, which are the two most widely adopted models by the community, in two major aspects: (i) the applicability of the TFE expression therein is extended to near-zero surface electric fields by an error-function correction, allowing for the calculation of the total current by a nontrivial sum of TE (over-the-barrier current) and TFE (below-the-barrier current) contributions; therefore, an accurate description of the TE-to-TFE transition region is captured analytically for the first time; (ii) image-force lowering is considered with much-simpler correction terms. Comparisons with the reference numerical model show that the unified TE–TFE model has excellent accuracy, as well as a 10 000× reduction in computation time. The unified model is further tested against experimental data from Schottky barrier diodes based on Si, 4H-SiC, GaN, and β-Ga_2O_3, revealing accurate extractions of barrier heights and correct descriptions of the ideal reverse leakage characteristics. With the extended applicable range, improved accuracy, and computational efficiency, the unified TE–TFE model is highly valuable for the design and analysis of devices based on Schottky junctions, as well as for potential integration in technology computer-aided design (TCAD) tools.

INTRODUCTION

The reverse-bias, i.e., leakage, current (J_R) in a Schottky junction bears crucial importance for many device applications. For example, it can determine the practical blocking voltage of a power Schottky barrier diode (SBD), especially for wide-bandgap (WBG) semiconductors.[1] It can also induce premature gate breakdown in metal–semiconductor field-effect transistors (MESFETs) and high electron mobility transistors (HEMTs)[2] and affect the responsivity of Schottky photodiodes.[3] In addition, the ideality of J_R provides important feedback on the interface and material quality. Therefore, accurate modeling of the ideal J_R in Schottky junctions is precious.

s partly illustrated in Fig. 1, there are three current mechanisms to consider in calculating the ideal leakage current of a SBD under reverse bias: thermionic emission (TE) that captures the over-the-barrier current, thermionic-field emission (TFE) that captures the below-the-barrier tunneling current under low-to-moderate surface electric fields, and field emission (FE, commonly calculated by the Fowler–Nordheim formula, not explicitly shown in Fig. 1) that captures the below-the-barrier tunneling current under high surface electric fields. The dominant reverse leakage mechanism in ideal Schottky junction transitions from TE to TFE and, finally, to FE, as temperature (T) decreases and/or the surface electric field (E) at the Schottky interface increases.[4] While a TE model with image-force lowering (IFL) is typically sufficient for Si SBDs,[5] TFE or even FE needs to be considered additionally in WBG SBDs,[1] since the surface electric field can be much higher than the surface field in Si SBDs.

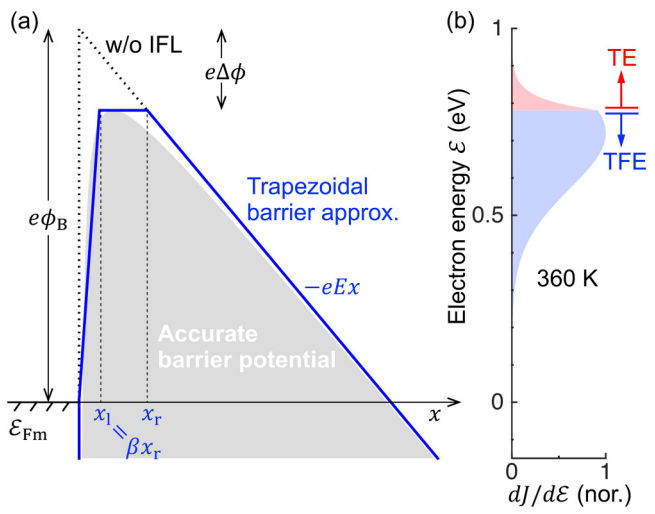

FIG. 1. (a) Trapezoidal barrier approximation used in our new TFE model for image-force lowering (IFL), involving a single empirical barrier-shape parameter β. (b) Current density per unit energy ($dJ/d\mathcal{E}$) calculated numerically based on the accurate barrier potential, showing contributions from both TE and TFE.

Multiple TFE models have been developed in the past, the ones most widely accepted and used being Murphy–Good[4] and Padovani–Stratton[6] TFE models, as well as Hatakeyama and Shinohe's simplified TFE model.[7] However, as will be discussed further in the next section, these existing TFE models are not applicable at low surface electric fields, where TE is the dominant reverse leakage mechanism. Hence, with the existing TE and TFE models, the total current can only be taken as *either* the TE current at low fields *or* the TFE current at moderate fields where the lower and upper bounds of the field need to be carefully determined. Hence, the current where both TE and TFE components are appreciable, i.e., the transition region, cannot be calculated analytically with high accuracy. In addition, the treatment of IFL in these models is either too complicated[4] or absent.[6,7]

These deficiencies motivate us to develop a unified TE–TFE analytical model with the following key features, allowing for the calculation of the total current by a non-trivial sum of the TE and TFE currents:

(i) Applicability at near-zero surface electric fields by introducing an *erfc* correction.
(ii) Proper treatment of IFL with simpler correction terms by introducing a single barrier-shape parameter β.
(iii) A typical reduction of 10^4 in the computation time in comparison to numerical calculations.

These features suggest that our unified TE–TFE analytical model can enable facile and accurate device designs and analysis, as well as significantly improve the performance of technology computer-aided design (TCAD) tools.

LIMITATIONS IN EXISTING TFE MODELS

Murphy–Good models

The first comprehensive analytical treatment of all three major reverse leakage mechanisms (TE, TFE, and FE) was made by Murphy and Good.[4] While Murphy–Good models agree well with the numerical model,[1,8] *no solution* is provided for the TE–TFE transition region, where neither the TE nor the TFE model is applicable [see Fig. 1(c) of Ref. 8].

Image-force lowering (IFL) is an important effect on J_R. While IFL is explicitly considered in Murphy–Good models, the image-force (IF) correction functions are very complicated[9] and can only be determined iteratively in the case of TFE.[4]

Padovani–Stratton models

Although IFL is considered in Murphy–Good models, the doping effect in the semiconductor is not included. Padovani and Stratton derived a TFE model that includes the doping effect;[6] however, IFL is not considered. Another limitation of the Padovani–Stratton model is that it is not applicable at a low surface electric field/reverse bias, where TE dominates.

Common mistakes in using TFE models

Both Murphy–Good and Padovani–Stratton TFE models are only applicable within a certain surface electric field (E) range, necessitating the use of appropriate conditions for *both the lower and upper limits of E*. However, they are rarely considered in practice, especially, the lower E limit. The same applies to Hatakeyama and Shinohe's simplified TFE model,[7] which is essentially identical

TABLE I. Comparison of different models for TFE.

	Image-force lowering	Applicable at $E \to 0$	Closed-form expression	Doping effect[a]
Murphy–Good TFE[4]	Yes[b]	No	Yes	No
Padovani–Stratton TFE[6]	No	No	Yes	Yes
TFE w/o IFL[7]	No[c]	No	Yes	No
Numerical model[1]	Yes	Yes	No	Yes
This work	Yes	Yes	Yes	No

[a]Insignificant below $\sim 1 \times 10^{18}$ cm^{-3}.
[b]Complex IF correction terms.
[c]Essentially, the Murphy–Good TFE model but without IF correction.

to the Murphy–Good TFE model with the IF correction terms neglected (henceforth, also referred to as *TFE without IFL*).

Another common mistake is the improper consideration of IFL in the TFE models by replacing ϕ_B with $\phi_B - \Delta\phi$, where ϕ_B is the barrier height and $\Delta\phi$ is the IFL. As illustrated in our previous work,[1] this would severely overestimate J_R. Such a mistake may be partially related to the IF correction being either too complicated (as in Murphy–Good TFE model) or absent (as in Padovani–Stratton and Hatakeyama–Shinohe TFE models). The limitations and features of the existing TFE models are summarized in Table I.

UNIFIED TE–TFE MODEL

To avoid the complicated IF correction terms as in the Murphy–Good TFE model due to the exact form of the IF potential, we employ a trapezoidal barrier approximation to the accurate barrier potential for calculation of the TFE current, as shown in Fig. 1(a). The same with the accurate barrier potential, the trapezoidal barrier has a barrier height of $\phi_B - \Delta\phi$, where ϕ_B is the barrier height without IFL and $\Delta\phi = \sqrt{eE/(4\pi\varepsilon_r\varepsilon_0)}$ is the image-force lowering, with ε_r being the relative dielectric constant for IFL. The trapezoidal barrier can be dissected into two triangular barriers and one rectangular barrier, for which the Wentzel–Kramers–Brillouin (WKB) tunneling probabilities all have simple analytical forms. A *single empirical parameter* β is used to adjust the barrier shape. As shown in Fig. 1(a), β is defined as the ratio between x_l (the x coordinate of the interface between the left triangular barrier and the rectangular barrier) and x_r (the x coordinate of the interface between the right triangular barrier and the rectangular barrier), where the metal–semiconductor interface defines the origin of the x axis. By numerically calculating the tunneling current under the trapezoidal barrier approximation and comparing with the results without barrier-shape approximation, we confirm this approximation can reproduce the IFL effect accurately with a proper β value in most cases (see later discussions).

The tunneling current flux is determined by the Fermi statistics and the transparency of the tunneling barrier.[4,6] As a result, the energy profile of the tunneling current density per unit energy ($dJ/d\mathcal{E}$) resembles a Gaussian distribution and exhibits a peak at certain electron energy ($\mathcal{E}$), which we define as $\mathcal{E}_0$. In the case of TFE, $\mathcal{E}_0$ lies in between the top of the barrier ($e\phi_B - e\Delta\phi$) and the metal Fermi-level energy ($\mathcal{E}_{Fm}$). As the surface electric field decreases, the barrier becomes less transparent to tunneling, therefore, $\mathcal{E}_0$ increases toward the top of the barrier and vice versa. In the derivation of the existing TFE expressions,[4,6] the energy profile of $dJ/d\mathcal{E}$ is approximated as a Gaussian distribution, and the upper limit of the integration is extended to $\mathcal{E} = +\infty$. This would necessitate the use of appropriate conditions for the lower limit of the surface electric field E. Otherwise, the integration of $dJ/d\mathcal{E}$ would artificially include some contributions of the current from electrons having energies above the top of the barrier.

To properly extend the applicability of the expression for TFE to near-zero surface electric fields, i.e., $E \to 0$, without the need of a condition on the aforementioned lower E limit, the integration of the tunneling current density per unit energy ($dJ/d\mathcal{E}$) as a function of electron energy ($\mathcal{E}$) should be limited to below the top of the barrier, as shown in Fig. 1(b). Apart from the trapezoidal barrier approximation, this is another important distinction in the derivation of our new TFE expression.

Main equations

By using the methods described above, we developed a new expression for the TFE current (J_{TFE}) for the unified TE–TFE model

$$J_{TFE} = J_0 \exp\left(\frac{\gamma e\Delta\phi}{k_B T}\right)\left(\frac{2\sqrt{\pi}\theta E}{E_0}\right)\exp\left(\frac{\theta^2 E^2}{3E_0^2}\right)\cdot\left[1 - \frac{1}{2}\mathrm{erfc}\left(\frac{\theta E}{2E_0}\right)\right]. \tag{1}$$

Here, $J_0 = A^* T^2 \exp[-e\phi_B/(k_B T)]$ is the saturation current, where A^* is the Richardson constant; $E_0 = 2\sqrt{2m_t}(k_B T)^{\frac{3}{2}}/(e\hbar)$ is the characteristic electric field, where m_t is the tunneling effective mass; γ and θ are dimensionless IF correction terms, as defined by

$$\gamma = \frac{\beta\phi_B}{\phi_B - (1-\beta)\Delta\phi} \tag{2}$$

and

$$\theta = 1 - \frac{\beta\Delta\phi}{\phi_B - (1-\beta)\Delta\phi}, \tag{3}$$

respectively. The definitions of β, ϕ_B, $\Delta\phi$, and E are also illustrated in Fig. 1(a). The derivation process can be found in the Appendix.

The new J_{TFE} expression in the unified TE–TFE model bears a similar functional form with the Murphy–Good TFE model [Eq. (75) in Ref. 4] but with two major differences: (i) the aforementioned integration limit leads to an additional erfc correction term; (ii) γ and θ are the new IF correction terms, both of which have significantly simpler form and are basic functions of β. When $\Delta\phi$ is not significant compared with ϕ_B, γ is approximately equal to β as from Eq. (2). On the other hand, the definition of θ arises from the reduced electric field due to the electric field associated with the left triangular barrier [see the Appendix and Fig. 1(a)]. Consequently, we have $\gamma \approx \beta < 1$ and $\theta < 1$. Since γ directly acts on the exponential term due to IFL in Eq. (1), the direct impact of $\Delta\phi$ on TFE is smaller than on TE. In addition, as $\theta < 1$ acts on the surface electric E, the effect of IFL on the electric-field dependence is further damped, highlighting the importance of a proper treatment of IFL in calculating the TFE current.

When IFL is ignored or not considered, both β and $\Delta\phi$ should be set to zero. In this case, the new J_{TFE} expression reduces to Hatakeyama–Shinohe simplified TFE model [Eq. (3) in Ref. 7], i.e., the TFE without IFL model referred in this work, except for the erfc correction, which simplifies to $1 - (1/2)\mathrm{erfc}[E/(2E_0)]$ under no IFL. It should be noted that the *erfc correction is present irrespective of IFL* or the trapezoidal barrier approximation we used, thus should be always included. This is one of the major contributions from this work.

Since the new J_{TFE} expression with the erfc correction only considers the below-the-barrier tunneling current and thus is applicable at near-zero surface electric field ($E \to 0$), the total reverse leakage current in the TE and TFE regime is simply a sum of the

TFE current (below-the-barrier current only) and the TE current (J_{TE}, over-the-barrier current only), i.e.,

$$J_R = J_{TE} + J_{TFE}, \tag{4}$$

where J_{TE} is given by the familiar expression

$$J_{TE} = J_0 \exp\left(\frac{e\Delta\phi}{k_B T}\right). \tag{5}$$

We emphasize that Eq. (4) is *not* trivial, as previous TFE models are never meant to/should not be used in conjunction with the TE model due to the inapplicability at near-zero surface electric fields. It is only after our introduction of the erfc correction in Eq. (1) that the TE current can be added to the TFE current.

Empirical compact model for the barrier-shape parameter β

The barrier-shape parameter β controls the transparency of the tunneling barrier seen by the tunneling electrons, thus can fine-tune the effect of IFL in the new TFE expression [Eq. (1)]. The optimum values of β are first obtained from optimization against the reference numerical model. As described in Ref. 1, the reference numerical model is based on numerical calculation of the WKB tunneling probability across the Schottky barrier considering the accurate barrier potential under image-force lowering [Fig. 1(a)]. Figure 2 shows the optimum values of β, which is primarily a function of ε_r, m_t and ϕ_B. Under a stronger effect of IFL, a larger β is needed. Correspondingly, β increases with decreasing ε_r. Similar, as the relative effect of IFL on a small barrier height is larger than on a large barrier height, β increases with decreasing ϕ_B. The dependence of β on m_t is less intuitive. As m_t decreases, the electron energy $\mathcal{E}_0$ at the peak value of $dJ/d\mathcal{E}$ decreases toward the Fermi-level energy $\mathcal{E}_{Fm}$, thus the effect of IFL is reduced. Therefore, β decreases with decreasing m_t, as shown in Fig. 2(a).

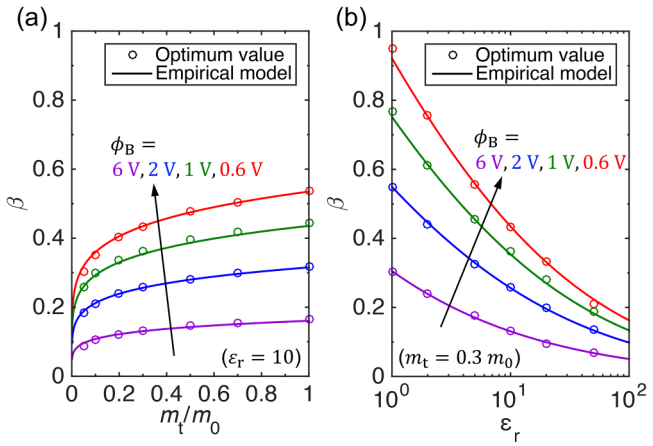

FIG. 2. Optimum β values as a function of (a) the tunneling effective mass (m_t) and (b) the relative dielectric constant (ε_r).

TABLE II. Parameter set of the empirical compact model for the barrier-shape parameter β.

a_0	a_1	a_2	b_0	b_1	b_2
0.7519	−0.4214	−0.0456	−0.2719	−0.0059	−0.0011
c_0	c_1		η_0		
−0.0233	0.0023	…	0.1724	…	…

The dependence of β on ε_r, m_t, and ϕ_B is found to be nearly uncorrelated, thus a simple empirical expression for β is obtained. With the introduction of a dimensionless barrier height parameter $\Phi_B = \phi_B/1\ \text{V}$, the empirical expression for β is given by

$$\beta(\varepsilon_r, \Phi_B, m_t) = \min\left\{\mathcal{A}\varepsilon_r^{\mathcal{B}} \exp[\mathcal{C}\cdot(\ln\varepsilon_r)^2]\left(\frac{m_t}{0.3m_0}\right)^{\eta_0}, 1\right\}, \tag{6}$$

where

$$\mathcal{A}(\Phi_B) = a_0\Phi_B^{a_1}\exp[a_2(\ln\Phi_B)^2], \tag{7}$$

$$\mathcal{B}(\Phi_B) = b_0 + b_1\Phi_B + b_2\Phi_B^2, \tag{8}$$

$$\mathcal{C}(\Phi_B) = c_0 + c_1\Phi_B. \tag{9}$$

The parameter set (a_0, a_1, a_2, b_0, b_1, b_2, c_0, c_1, η_0, total of 9 parameters) is obtained from fitting the empirical expression [Eqs. (6)–(9)] to the optimum values of β, as summarized in

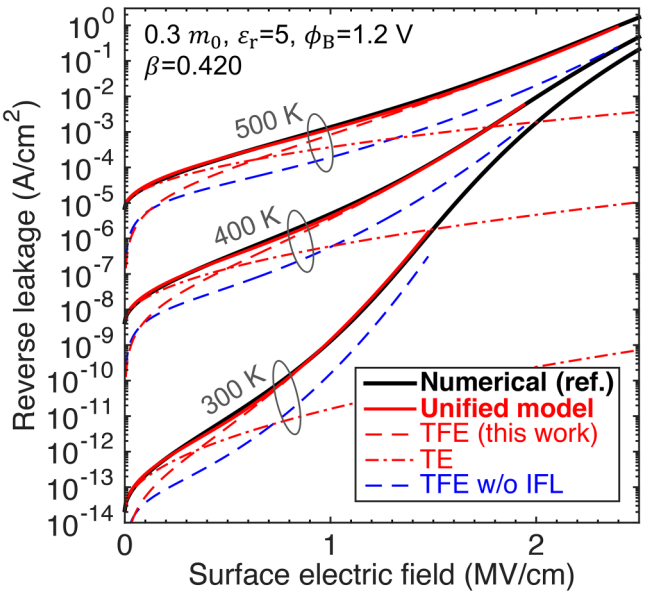

FIG. 3. Verification of the unified model against the reference numerical model.[1] Excellent agreement is achieved throughout the entire TE and TFE regimes.

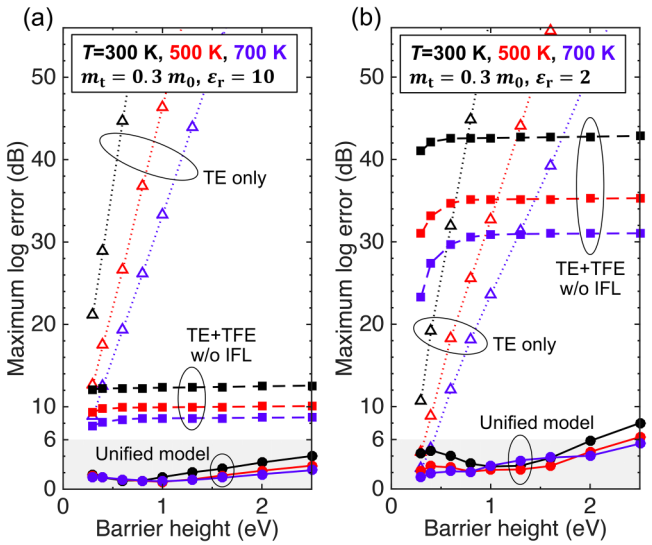

FIG. 4. The maximum log error ($|20\log_{10}(J_R/J_{R,ref})|$) relative to the reference numerical model ($J_{R,ref}$) at (a) $\varepsilon_r = 10$ and (b) $\varepsilon_r = 2$. The unified TE–TFE model (solid circles) shows significantly better accuracy than either the TE model alone (hollow triangles) or the unified model itself but without IFL, i.e., $\beta = 0$ and $\Delta\phi = 0$ (solid squares). $m_t = 0.3\ m_0$; the erfc correction is also applied to the TFE without IFL for best accuracy.

Table II. Very good match between the optimum β values and the empirical expression is obtained throughout an entire range of $\varepsilon_r \in [1, 50]$, $\phi_B \in [0.6, 6\,\text{V}]$, and $m_t/m_0 \in [0.05, 1]$, as partially illustrated in Fig. 2. With the parameter set determined and verified, Eqs. (6)–(9) serve as a compact model for β.

For $\phi_B < 0.6\,\text{V}$, we found that the compact model for β becomes less accurate with respect to the optimum β values. However, these less accurate β values impart no appreciable impact on the accuracy of J_R, thus the compact model for β is still applicable under $\phi_B < 0.6\,\text{V}$. Similarly, the applicable tunneling effective mass can be extended to $<0.05\ m_0$, and the applicable ε_r can be extended to $+\infty$.

Consequently, *the applicability range of the compact model for* β is $\varepsilon_r \in [1, +\infty)$, $\phi_B \in (0, 6\,\text{V}]$ and $m_t/m_0 \in (0, 1]$. Outside of this range, the compact model can *still* be used; however, the accuracy of the calculated J_R may decrease. We will discuss the accuracy of J_R in a later section.

Conditions for the upper limit of *E*

When the surface electric field E increases beyond a certain value, TFE transitions into FE, at which point the TFE model is no longer valid. Therefore, it is important to find conditions for the upper E limit ($E_{u,lim}$) of TFE. By using the method described in Ref. 4, we derived the conditions for $E_{u,lim}$ of the unified TE–TFE model (see the Appendix for the derivation), which is imparted by the applicability conditions of the new J_{TFE} expression [Eq. (1)]

$$\left(\frac{1+\sqrt{1-3a_E b_E}}{3b_E}\right)^2 + \left(\frac{3b_E}{2}t_F^{\frac{1}{2}} + \frac{a_E}{2}t_F^{-\frac{1}{2}} - 1\right)^{-1} < t_F - 1 \quad (10)$$

and

$$\frac{3b_E}{2}t_F^{\frac{1}{2}} + \frac{a_E}{2}t_F^{-\frac{1}{2}} - 1 > 0\,, \quad (11)$$

where the abbreviations are defined as

$$a_E = (1-\beta)\left(\frac{e\Delta\phi}{k_B T}\right)\frac{E_0}{E}, \quad (12)$$

$$b_E = \frac{2}{3\theta}\left(\frac{E_0}{E}\right), \quad (13)$$

$$t_F = \frac{e(\phi_B - \Delta\phi)}{k_B T}. \quad (14)$$

These conditions are found to yield near-identical values of the upper E limit compared with those calculated from the upper E limit condition in the Murphy–Good TFE model [Eq. (69) in Ref. 4].

TABLE III. Accuracy of the unified model under different conditions with respect to the reference numerical model, evaluated within a temperature range of [300, 700 K] and an electric-field range of $(0, E_{u,lim}]$.

Minimum ε_r	Maximum m_t/m_0	Maximum ϕ_B (V)	Accurate to within a factor of	Maximum log error ($\lvert 20\log_{10}(J_R/J_{R,ref})\rvert$) (dB)
10	4	2	1.9	5.8
5	3.5	2	2.0	6.0
5	1	2.5	2.3	7.3
5	1	3	2.8	8.8
2	0.6	2	2.0	6.0
2	1	2.5	2.6	8.2
2	1	3	3.4	10.5
1	1	3	4.2	12.6
1	1	5	9.5	19.5
1	1	6	14.7	23.4

For simplicity, a relaxed condition is also derived,

$$\frac{E}{E_0} < \sqrt{\frac{e\phi_B}{k_B T}}. \tag{15}$$

This expression is identical to Padovani and Stratton's condition.[6] It can be shown that Eq. (15) slightly overestimates the upper limit of E in comparison with the rigorous conditions [Eqs. (10) and (11)].

VALIDATION OF THE UNIFIED TE–TFE MODEL

To verify the accuracy of the unified TE–TFE model [Eqs. (1)–(14)], we calculate J_R as a function of the surface electric field E and temperature T within $E \in (0, E_{u,lim}]$ and compare the results with the values obtained from the reference numerical model ($J_{R,ref}$).[1] It can be seen from Fig. 3 that the unified model not only exhibits excellent agreement with the reference numerical model but also covers the entire TE/TFE regime, including the transition region, where the transition electric field resides.[8] The calculations from TFE without IFL, i.e., Hatakeyama and Shinohe's simplified TFE model,[7] are also shown as a comparison, highlighting the importance of IFL. A full comparison with other models is summarized in Table I. Although the present model neglects the doping effect, it is still broadly applicable, especially for high-voltage devices, since the doping effect is found to be insignificant for net doping concentrations lower than $\sim 1 \times 10^{18}$ cm^{-3}.

To quantify the accuracy of the unified TE–TFE model, the maximum log error with respect to the reference numerical model ($|20\log_{10}(J_R/J_{R,ref})|$) is calculated within the entire applicable range of the surface electric field, i.e., $E \in (0, E_{u,lim}]$. The results are shown in Fig. 4 as a function of the barrier height. The unified model has much smaller errors than either the TE model alone or the unified model itself but without IFL ($\beta = 0$ and $\Delta\phi = 0$), especially when IFL is prominent as in the case of a small ε_r. We found that the log error is larger with smaller ε_r, larger m_t, and larger ϕ_B. Specifically, within a parameter space of $\varepsilon_r \geq 2$, $m_t/m_0 \leq 0.6$, $\phi_B \leq 2$ V, and a T range of 300–700 K, which encompass the common scenarios of most semiconductor SBDs, the unified model is accurate to within a factor of 2 (6 dB).

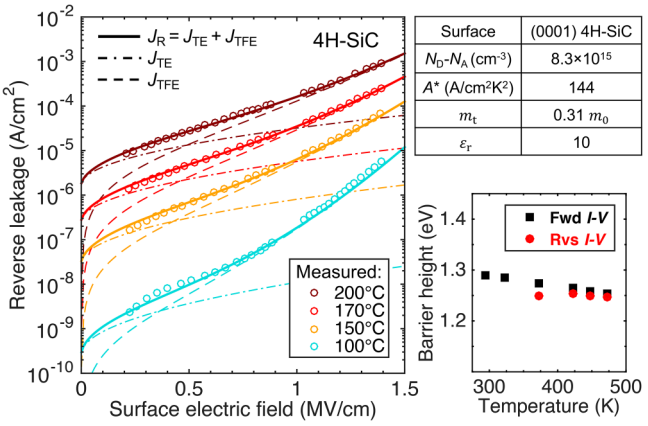

FIG. 5. Analysis of near-ideal reverse leakage characteristics in 4H-SiC SBDs[11] using the unified TE–TFE model, *with the barrier height as the only fitting parameter* (the same for Figs. 6–8). The net doping concentration $N_D - N_A$ is calculated based on the estimated surface electric field of 1.35 MV/cm at 600 V reverse bias.[11] The Richardson constant A^* and the tunneling effective mass m_t along the (0001) direction are calculated based on the methods in Ref. 15 by using the theoretical effective mass tensor in Ref. 16. These values agree with those used in Ref. 17. The relative dielectric constant ε_r is based on the values from Refs. 17 and 18. The extracted barrier height values agree well with extraction from forward current–voltage (I–V) characteristics.

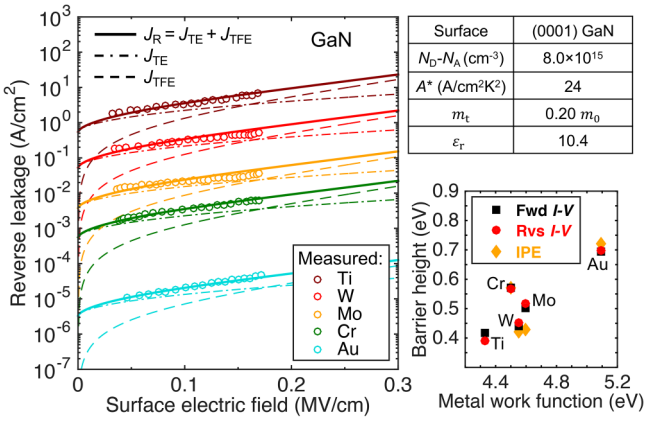

FIG. 6. Analysis of near-ideal reverse leakage characteristics at room temperature in GaN SBDs with different Schottky metal contacts.[12] $N_D - N_A$ is taken from Fig. 1(b) in Ref. 12; A^* and m_t along the (0001) direction are calculated based on the methods in Ref. 15 by using the effective mass value in Ref. 19; ε_r is taken from Ref. 20. The extracted barrier heights agree well with values obtained from forward I–V and Internal Photoemission (IPE) methods.[12]

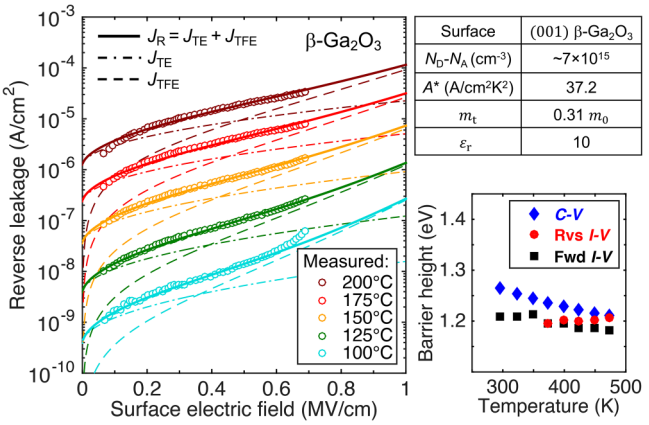

FIG. 7. Analysis of near-ideal reverse leakage characteristics in β-Ga_2O_3 SBDs.[8] $N_D - N_A$ is extracted from capacitance–voltage (C–V) profiling in Ref. 8; A^* and m_t are based on the experimentally measured electron effective mass;[21] ε_r is taken from Ref. 22. The extracted barrier heights agree well with values obtained from forward I–V and C–V methods.

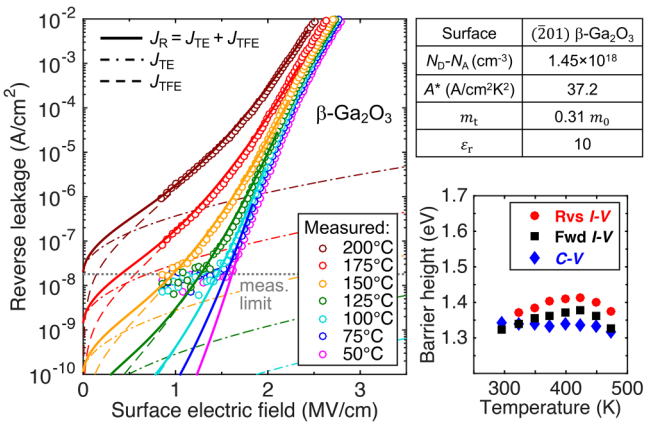

FIG. 8. Analysis of near-ideal reverse leakage characteristics in β-Ga_2O_3 SBDs with a high net doping concentration.[1] $N_D - N_A$ is extracted from *C–V* profiling in Ref. 1; A^* and m_t are based on the experimentally measured electron effective mass;[21] ε_r is taken from Ref. 22. The extracted barrier heights are slightly higher than from other methods due to the doping effect, which is not considered in the unified TE–TFE model.

We also calculated the accuracy of the unified TE–TFE model within multiple other parameter spaces in an effort to cover different scenarios of TE/TFE as much as possible. The results are summarized in Table III. It is worth noting that the unified model can even be applied to TE and TFE of metals to vacuum ($\varepsilon_r = 1$, $m_t/m_0 = 1$, $2\,\text{V} \le \phi_B \le 6\,\text{V}$),[10] although the accuracy is worse than typical cases of semiconductor SBDs.

APPLICATION TO EXPERIMENTAL DATA

The accuracy and applicability of the unified model are further tested by fitting to the experimental data on near-ideal SBDs. First, we perform the fitting on wide-bandgap SBDs based on 4H-SiC[11] (Fig. 5), GaN[12] (Fig. 6), and β-Ga_2O_3[1,8] (Figs. 7 and 8). The barrier height is used as the only fitting parameter, while all other parameters are determined from either independent experiments or theoretical calculations. The dielectric constants for IFL are assumed to be identical to the static values. This assumption is found to be valid in Si[13] but requires further scrutiny otherwise.[14]

In general, we find excellent agreement between the experimental data and the unified model on moderately doped WBG materials, as shown in Figs. 5–7. The extracted barrier heights are closely matched with values obtained from other methods. Furthermore, the transition between TE and TFE dominated regimes is well captured by the unified model, highlighting the power of the unified TE–TFE model, which was made possible by the usage of the erfc correction to the TFE expression. There exists a slight deviation in the 100 °C experiment data from the model at a high surface electric field in Fig. 7. It is due to the residue edge leakage current not fully suppressed by the field plate of the device (see discussions in Ref. 8).

For heavily doped materials (Fig. 8), the agreement between the experimental data and the unified model is still very good. However, the extracted ϕ_B values are slightly higher than the values from other extraction methods due to the doping effect, which is not considered in the unified TE–TFE model presented here. It is worth noting that the experimental data were measured to surface electric field values higher than the upper E limit ($E_{u,lim}$) of TFE [Eqs. (10)–(14)]. Thus, the unified model is only able to fit to the

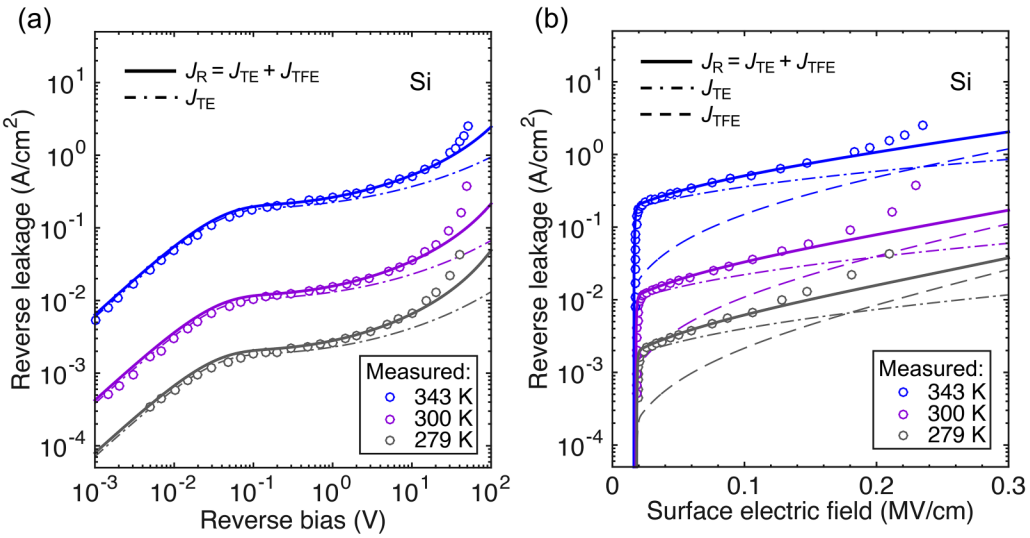

FIG. 9. Analysis of near-ideal reverse leakage characteristics in Si SBDs:[23] (a) reverse leakage current *vs* reverse bias; (b) reverse leakage current *vs* surface electric field. The net doping concentration (3.5×10^{15} cm^{-3}), the effective Richardson constant (112 A/cm^2 K^2), and the barrier height value (0.55 eV) are all adopted from Ref. 23. The effects of optical photon scattering and quantum-mechanical reflection are considered in the calculation of the effective Richardson constant.[23] ε_r for IFL is taken to be 11.7, the same as the static value, while the tunneling effective mass along the [111] transport direction is calculated to be 0.26 m_0 according to Ref. 15. Therefore, no fitting is involved in the calculations.

range of surface electric field within (0, $E_{u,lim}$], beyond which field emission models should be used.

It is important to note that the applicability of the unified TE–TFE is not limited to SBDs based on WBG materials. To illustrate this, we performed data analysis using the unified TE–TFE model on near-ideal Si SBDs,[23] as shown in Fig. 9. Here, to accurately capture the voltage-dependence of the saturation current J_0 in the low reverse bias (V_R) region, the familiar factor $[1 - \exp(-eV_R/k_BT)]$ is applied to J_0 in the unified TE–TFE model.[23] As this factor quickly approaches unity when V_R is beyond a few times the thermal voltage k_BT/e, it is generally neglected, especially, in the case of WBG SBDs, where the breakdown voltage is typically more than two orders of magnitude higher than the thermal voltage.

It can be seen that the unified TE–TFE model again shows excellent agreement to the reverse leakage characteristics on Si SBDs. Although not the dominant process, the incorporation of the TFE contribution in the unified model facilitates better agreement with experimental data compared with TE model alone, without needing to invoke an additional barrier lowering mechanism due to surface dipole.[23] Beyond a reverse bias of ~30 V or a surface electric field of ~0.18 MV/cm, the deviation between the unified TE–TFE model and the experimental data is largely due to the initiation of avalanche multiplication due to impact ionization.[23]

CONCLUSIONS

A unified TE–TFE analytical model, TE for over-the-barrier current and TFE for below-the-barrier current, is developed for the ideal Schottky reverse leakage current for the first time [Eqs. (1), (4) and (5)]. The unified TE–TFE analytical model allows one to simply sum the TE and TFE current contributions [Eq. (4)] to calculate the total current. The new TFE model therein [Eq. (1)] possesses two unprecedented features: much simplified image-force correction terms and applicability at near-zero surface electric field, which are enabled by a single empirical barrier-shape parameter β and an error-function correction, respectively. A simple compact model for β is provided [Eq. (6)], valid for a wide range of material parameters: $\varepsilon_r \in [1, +\infty)$, $\phi_B \in (0, 6\,V]$, and $m_t/m_0 \in (0, 1]$.

The unified TE–TFE model is verified against numerical calculations across a wide temperature range of 300–700 K and the entire applicable range of the surface electric field, i.e., $E \in (0, E_{u,lim}]$, with $E_{u,lim}$ being the upper E limit of the TFE regime [Eqs. (10) and (11)]. An accuracy of a factor of 2 or better is confirmed in all common cases of semiconductor SBDs. Fitting against experimental data on Si, 4H-SiC, GaN, and Ga_2O_3 SBDs shows excellent accuracy across the entire TE and TFE regime—a feat not possible with the existing TFE models prior to this work. In addition, we find that the unified TE–TFE model shows a 10^4-fold reduction in typical computation time compared with the numerical model.[1] These features make the unified TE–TFE model highly valuable for the design and analysis of a variety of devices based on Schottky junctions. Finally, the unified TE–TFE model can be implemented easily in TCAD tools due to the absence of nonlocal dependence on the electric field. Consequently, one can anticipate significant advantages in both computational efficiency and convergence against typical nonlocal tunneling models.

ACKNOWLEDGMENTS

The authors are thankful for the support from ULTRA (analytical modeling), an Energy Frontier Research Center funded by the U.S. Department of Energy (DOE), Office of Science, Basic Energy Sciences (BES), under Award No. DE-SC0021230. The work is also supported, in part, by the Air Force Office of Scientific Research (AFOSR) (No. FA9550-20-1-0148, numerical modeling), ComSenTer (experimental validation), one of the six SRC JUMP centers, and ACCESS (Ga_2O_3 SBDs), an AFOSR Center of Excellence (No. FA9550-18-1-0529).

AUTHOR DECLARATIONS

Conflict of Interest

The authors have no conflicts to disclose.

DATA AVAILABILITY

The data that support the findings of this study are available within this article.

APPENDIX: DERIVATION OF THE NEW TFE EXPRESSION UNDER TRAPEZOIDAL BARRIER APPROXIMATION

The barrier tunneling current under reverse bias is given by[4,8]

$$J_{BT} = \frac{A^*T}{k_B}\int_{-\infty}^{e\phi'_B} \mathcal{T}(\mathcal{E}) \cdot \ln\left[1 + \exp\left(-\frac{\mathcal{E} - \mathcal{E}_{Fm}}{k_BT}\right)\right] d\mathcal{E}, \quad \text{(A1)}$$

where $\mathcal{T}(\mathcal{E})$ is the tunneling probability, $\mathcal{E}$ is the electron energy incident on the barrier (i.e., with the transverse kinetic energy excluded),[4] $\mathcal{E}_{Fm}$ is the metal Fermi-level energy, and $\phi'_B = \phi_B - \Delta\phi$ is the barrier height under image-force lowering. Equation (A1) only considers electron tunneling from the metal to the semiconductor and neglects that from the semiconductor to the metal. This is a valid assumption when the reverse bias is beyond a few times the thermal voltage k_BT/e. With our trapezoidal barrier approximation, the tunneling barrier can be dissected into a left triangular barrier, a rectangular barrier, and a right triangular barrier [Fig. 1(a)], for which the WKB tunneling probabilities [$\mathcal{T}_1(\mathcal{E})$, $\mathcal{T}_2(\mathcal{E})$, and $\mathcal{T}_3(\mathcal{E})$, respectively] all have simple analytical forms,

$$\mathcal{T}_1(\mathcal{E}) = \exp\left[-\frac{4\sqrt{2m_t}}{3eE_l\hbar}(e\phi'_B - \mathcal{E})^{\frac{3}{2}}\right], \quad \text{(A2)}$$

$$\mathcal{T}_2(\mathcal{E}) = \exp\left[-\frac{2\sqrt{2m_t}(x_r - x_l)}{\hbar}(e\phi'_B - \mathcal{E})^{\frac{1}{2}}\right], \quad \text{(A3)}$$

$$\mathcal{T}_3(\mathcal{E}) = \exp\left[-\frac{4\sqrt{2m_t}}{3eE\hbar}(e\phi'_B - \mathcal{E})^{\frac{3}{2}}\right], \quad \text{(A4)}$$

where $E_l = \frac{\phi_B - \Delta\phi}{x_l}$ is the electric field associated with the left triangular barrier. $\mathcal{T}(\mathcal{E})$ is simply the product of the three individual

probabilities

$$T(\mathcal{E}) = \mathcal{T}_1(\mathcal{E}) \cdot \mathcal{T}_2(\mathcal{E}) \cdot \mathcal{T}_3(\mathcal{E}). \tag{A5}$$

In the TFE regime, $\mathcal{E} - \mathcal{E}_{Fm} > k_B T$, thus $\ln\left[1 + \exp\left(-\frac{\mathcal{E}-\mathcal{E}_{Fm}}{k_B T}\right)\right] \approx \exp\left(-\frac{\mathcal{E}-\mathcal{E}_{Fm}}{k_B T}\right)$. Define $t = \frac{e\phi'_B - \mathcal{E}}{k_B T}$ as a unitless representation of the electron energy, $\theta E = \frac{EE_i}{E+E_i}$ as the reduced surface electric field considering the effect of E_i, and use Eqs. (A1)–(A5), we get the expression of the TFE current

$$J_{TFE} = A^* T^2 \exp\left(-\frac{e\phi'_B}{k_B T}\right) \int_0^{+\infty} \exp\left(-b_E t^{\frac{3}{2}} - a_E t^{\frac{1}{2}} + t\right) dt, \tag{A6}$$

where a_E and b_E are defined in Eqs. (12) and (13), respectively. As discussed in Murphy and Good's work,[4] the integral can be approximately evaluated by the expansion of the first and second terms in the exponent to the second order about the peak of the integrand t_0. The integrand then becomes

$$\exp[-C_0 - C_1(t - t_0) - C_2(t - t_0)^2 + t], \tag{A7}$$

where

$$t_0 = \left(\frac{1 + \sqrt{1 - 3a_E b_E}}{3b_E}\right)^2, \tag{A8}$$

$$C_0 = b_E t_0^{\frac{3}{2}} + a_E t_0^{\frac{1}{2}}, \tag{A9}$$

$$C_1 = \frac{3b_E}{2} t_0^{\frac{1}{2}} + \frac{a_E}{2} t_0^{-\frac{1}{2}}, \tag{A10}$$

$$C_2 = \frac{3b_E}{8} t_0^{-\frac{1}{2}} - \frac{a_E}{8} t_0^{-\frac{3}{2}}. \tag{A11}$$

It can be shown that t_0 increases with increasing surface electric field E. This corresponds to the actual electron energy at the peak tunneling current flux decreasing with increasing surface electric field E, an expected trend. Let $t' = t - t_0$, the expression of the TFE current then becomes

$$J_{TFE} = A^* T^2 \exp\left(-\frac{e\phi'_B}{k_B T}\right) \exp\left[t_0 - C_0 + \frac{(C_1 - 1)^2}{4C_2}\right] \times \int_{-t_0}^{+\infty} \exp\left[-C_2\left(t' + \frac{C_1 - 1}{2C_2}\right)^2\right] dt'. \tag{A12}$$

One can recognize the integral as a Gaussian integral. In Murphy–Good and Padovani–Stratton's treatments,[4,6] the lower limit of the integral is extended to $-\infty$. This will artificially include some extra contribution to the tunneling current from electrons having energies above the top of the barrier, necessitating careful calculation of the lower limit of the surface electric field when using these existing TFE models. To avoid this, we retain the lower limit of the integral $(-t_0)$ throughout the evaluation of the integral. This is equivalent to retaining the upper limit of integral $(e\phi'_B)$ in the original expression [Eq. (A1)], ensuring that only below the barrier tunneling flux is included and improving the accuracy of the model at near-zero surface electric fields.

Expanding the expressions of t_0, C_0, C_1, and C_2 in terms of $3a_E b_E$ and neglecting higher order terms, Eq. (A12) can be evaluated, and the final result is Eq. (1). Note that the error-function correction in Eq. (1) is directly resulted from retaining the lower limit of the integral $(-t_0)$ in Eq. (A12).

Strictly speaking, the expansion of t_0, C_0, C_1, and C_2 in terms of $3a_E b_E$ requires that $3a_E b_E < 1$, which would eventually fail when the surface electric field E approaches zero since $3a_E b_E$ goes as $E^{-3/2}$. However, this does not present any difficulty in the final expression since Eq. (1) is well-behaved at $E \to 0$. Furthermore, we find that the total reverse leakage current $(J_{TE} + J_{TFE})$ calculated with our new TFE expression agrees well with the reference numerical model across expansive parameter spaces (see discussions on the accuracy of the unified TE–TFE model). This is because the thermionic emission current dominates the total reverse leakage current at the near-zero electric field. Consequently, the applicability of our new TFE expression can be safely extended to the near-zero electric field when used in conjunction with the TE model as in the unified TE–TFE model.

Finally, we discuss the derivation of the conditions for the upper limit of the surface electric field [Eqs. (10)–(14)]. At sufficiently high surface electric field, t_0 approaches the Fermi-level energy $\left(t_F = \frac{e\phi'_B}{k_B T}\right)$, at which point the approximation of Fermi–Dirac statistics with Maxwell–Boltzmann statistics would eventually fail. Following the method in Ref. 4, we expand the first and second terms in the exponent in Eq. (A6) to linear terms about the Fermi-level energy t_F such that the entire exponent of the integrand becomes

$$-C_{0,F} - C_{1,F}(t - t_F) + t \propto -(C_{1,F} - 1)t, \tag{A13}$$

where

$$C_{0,F} = b_E t_F^{\frac{3}{2}} + a_E t_F^{\frac{1}{2}}, \tag{A14}$$

$$C_{1,F} = \frac{3b_E}{2} t_F^{\frac{1}{2}} + \frac{a_E}{2} t_F^{-\frac{1}{2}}. \tag{A15}$$

To ensure that the integrand exponentially decays and becomes no longer appreciable at $\mathcal{E} - \mathcal{E}_{Fm} = k_B T$, i.e., $t = t_F - 1$, we have

$$t_0 + (C_{1,F} - 1)^{-1} < t_F - 1 \tag{A16}$$

and

$$C_{1,F} > 1. \tag{A17}$$

After plugging in Eqs. (A14) and (A15), we get the final conditions for the upper limit of the surface electric field [Eqs. (10)–(14)]. If image-force lowering is ignored and Eq. (A16)

is simplified to $t_0 < t_F$, the simplified relaxed condition [Eq. (15)] is arrived.

REFERENCES

[1]W. Li, D. Saraswat, Y. Long, K. Nomoto, D. Jena, and H. G. Xing, Appl. Phys. Lett. **116**, 192101 (2020).
[2]R. J. Trew and U. K. Mishra, IEEE Electron Device Lett. **12**, 524–526 (1991).
[3]O. Katz, V. Garber, B. Meyler, G. Bahir, and J. Salzman, Appl. Phys. Lett. **79**, 1417–1419 (2001).
[4]E. L. Murphy and R. H. Good, Jr., Phys. Rev. **102**, 1464–1473 (1956).
[5]B. J. Baliga, *Advanced Power Rectifier Concepts* (Springer Science & Business Media, New York, 2009), pp. 23–25.
[6]F. A. Padovani and R. Stratton, Solid-State Electron. **9**, 695–707 (1966).
[7]T. Hatakeyama and T. Shinohe, Mater. Sci. Forum **389–393**, 1169–1172 (2002).
[8]W. Li, K. Nomoto, D. Jena, and H. G. Xing, Appl. Phys. Lett. **117**, 222104 (2020).
[9]R. E. Burgess, H. Kroemer, and J. M. Houston, Phys. Rev. **90**, 515 (1953).
[10]H. B. Michaelson, J. Appl. Phys. **48**, 4729–4733 (1977).
[11]M. Treu, R. Rupp, H. Kapels, and W. Bartsch, Mater. Sci. Forum **353–356**, 679–682 (2001).
[12]H. Imadate, T. Mishima, and K. Shiojima, Jpn. J. Appl. Phys. **57**, 04FG13 (2018).
[13]S. M. Sze, C. R. Crowell, and D. Kahng, J. Appl. Phys. **35**, 2534–2536 (1964).
[14]S. M. Sze and K. K. Ng, *Physics of Semiconductor Devices* (Wiley, New York, 2007), pp. 148–149.
[15]C. R. Crowell, Solid-State Electron. **12**, 55–59 (1969).
[16]D. Volm, B. K. Meyer, D. M. Hofmann, W. M. Chen, N. T. Son, C. Persson, U. Lindefelt, O. Kordina, E. Sorman, A. O. Konstantinov, B. Monemar, and E. Janzen, Phys. Rev. B **53**, 15409–15412 (1996).
[17]M. Hara, S. Asada, T. Maeda, and T. Kimoto, Appl. Phys. Express **13**, 041001 (2020).
[18]T. Kimoto, Jpn. J. Appl. Phys. **54**, 040103 (2015).
[19]I. Vurgaftman, J. A. Meyer, and L. A. Ram-Mohan, J. Appl. Phys. **89**, 5815–5875 (2001).
[20]A. S. Barker, Jr. and M. Ilegems, Phys. Rev. B **7**, 743–750 (1973).
[21]Y. Zhang, A. Neal, Z. Xia, C. Joishi, J. M. Johnson, Y. Zheng, S. Bajaj, M. Brenner, D. Dorsey, K. Chabak, G. Jessen, J. Hwang, S. Mou, J. P. Heremans, and S. Rajan, Appl. Phys. Lett. **112**, 173502 (2018).
[22]B. Hoeneisen, C. A. Mead, and M.-A. Nicolet, Solid State Electron. **14**, 1057–1059 (1971).
[23]J. M. Andrews and M. P. Lepselter, Solid-State Electron. **13**, 1011–1023 (1970).